1-1-2014

A germanium/single-walled carbon nanotube composite paper as a free-standing anode for lithium-ion batteries

Jun Wang
University of Wollongong, jw707@uowmail.edu.au

Jiazhao Wang
University of Wollongong, jiazhao@uow.edu.au

Ziqi Sun
University of Wollongong, ziqi@uow.edu.au

Xuanwen Gao
University of Wollongong, xg973@uowmail.edu.au

Chao Zhong
University of Wollongong, cz527@uowmail.edu.au

See next page for additional authors

A germanium/single-walled carbon nanotube composite paper as a free-standing anode for lithium-ion batteries

Abstract

Paper-like free-standing germanium (Ge) and single-walled carbon nanotube (SWCNT) composite anodes were synthesized by the vacuum filtration of Ge/SWCNT composites, which were prepared by a facile aqueous-based method. The samples were characterized by X-ray diffraction, field emission scanning electron microscopy, and transmission electron microscopy. Electrochemical measurements demonstrate that the Ge/SWCNT composite paper anode with the weight percentage of 32% Ge delivered a specific discharge capacity of 417 mA h g−1 after 40 cycles at a current density of 25 mA g−1, 117% higher than the pure SWCNT paper anode. The SWCNTs not only function as a flexible mechanical support for strain release, but also provide excellent electrically conducting channels, while the nanosized Ge particles contribute to improving the discharge capacity of the paper anode.

Keywords

ion, lithium, anode, standing, carbon, batteries, free, germanium, single, paper, composite, nanotube, walled

Disciplines

Engineering | Physical Sciences and Mathematics

Publication Details

Wang, J., Wang, J., Sun, Z., Gao, X., Zhong, C., Chou, S. & Liu, H. (2014). A germanium/single-walled carbon nanotube composite paper as a free-standing anode for lithium-ion batteries. Journal of Materials Chemistry A: materials for energy and sustainability, 2 (13), 4613-4618.

Authors

Jun Wang, Jiazhao Wang, Ziqi Sun, Xuanwen Gao, Chao Zhong, Shulei Chou, and Hua-Kun Liu

Journal Name

RSCPublishing

ARTICLE

Germanium / Single-Walled Carbon Nanotube Composite Paper as a Free-Standing Anode for Lithium-ion Batteries

Cite this: DOI: 10.1039/xoxxoooooox

Received ooth January 2012,
Accepted ooth January 2012

DOI: 10.1039/xoxxoooooox

www.rsc.org/

Jun Wang[a,b], Jia-Zhao Wang[*a], Zi-Qi Sun[a], Xuan-Wen Gao[a], Chao Zhong[a], Shu-Lei Chou[a], Hua-Kun Liu[*a,b]

Paper-like free-standing germanium (Ge) and single-walled carbon nanotube (SWCNT) composite anodes were synthesized by the vacuum filtration of Ge/SWCNT composites, which were prepared by a facile aqueous-based method. The samples were characterized by X-ray diffraction, field emission scanning electron microscopy, and transmission electron microscopy. Electrochemical measurements demonstrate that the Ge/SWCNT composite paper anode with the weight percentage of 32% Ge delivered a specific discharge capacity of 417 mAh g^{-1} after 40 cycles at a current density of 25 mA g^{-1}, 117% higher than the pure SWCNT paper anode. The SWCNTs not only function as a flexible mechanical support for strain release, but also provide excellent electrically conducting channels, while the nanosized Ge contributes to improving the discharge capacity of the paper anode.

Introduction

Because of their environmental friendliness, large energy density, high operating voltage, and long cycling lifetime lithium-ion batteries (LIBs) have become one of the most heavily employed mobile energy sources in today's world [1,2]. Recently, consumer demand has been driving research efforts on small, thin, lightweight, and bendable LIBs to meet the various design and power needs of modern flexible electronic devices, such as roll-up displays, active radio-frequency identification tags, integrated circuit smart cards and implantable medical devices [3-5]. As an important part of LIBs, the anode consists of a metal substrate coated with a mixture of an active material, an electrical conductor, a binder, and a solvent. This type of anode is not suitable for flexible or bendable LIBs because it suffers from serious cracking and damage caused by the weak bonding between the metal substrate and the other materials during frequent bending. To avoid this drawback and lower the cost of LIBs, the development of free-standing anode materials is required [6,7].

The pure SWCNT paper anode has shown favourable flexibility and conductivity, and hence, is very suitable for producing free-standing anodes [8,9]. Current research to develop free-standing SWCNT paper anode takes advantage of its unique electronic and structural properties, such as light weight, high conductivity, good cycling stability, and high mechanical strength in lithium cells [10,11]. Although SWCNT paper anode has several advantages, its energy density is limited due to the low practical capacity. Therefore, the hybridization of an active second phase with SWCNTs is expected to introduce high capacity and good cycleability.

Composites with SWCNTs, such as Si/SWCNT [12,13], Fe_2O_3/SWCNT [14,15], SnO_2/SWCNT [16], and MnO_x/SWCNT [17] have been reported as paper anode materials. Although good electrochemical performances achieved by these already studied composite paper anodes were attractive, most of the preparation routes are too complicated or require high reaction temperature, limiting their industrial implementation. Therefore, it is of great interest to synthesize a new composite paper anode material by a green and efficient method at a low temperature.

Therefore, we designed and prepared a novel free-standing Germanium (Ge)/SWCNT composite paper anode based on the following ideas:

(i) SWCNTs could serve as a highly conductive and flexible matrix, which not only provides good electronic contact for the whole paper anode, but also effectively accommodates huge volume changes of the Ge particles during the cycling.

(ii) Ge as the electrochemically active second phase (1600 mAh g^{-1} theoretical capacity) could play an important role in improving the discharge capacity of the SWCNT composite paper anode. In addition, Germanium (Ge) has been intensively studied recently due to its 400 times faster lithium diffusivity and 104 times higher electrical conductivity than the commonly and widely studied silicon [18-20]. This makes it a promising candidate for composites with SWCNTs for use as a flexible anode.

(iii) Utilizing a simple and efficient method to fabricate a free-standing Ge/SWCNT composite paper without current collector and any binder could be useful for preparation of bendable batteries.

R. A. DiLeo's group [21] has reported a free-standing Ge/SWCNT anode prepared by depositing Ge onto SWCNT

paper using an electron-beam evaporation method, and the results show a stable discharge capacity within 10 cycles. This method may cause high energy consumption and present a safety risk, however. Moreover, the thin film anode with bilayer structure tends to suffer contact problems, and its electronic conductivity thus decreases, which leads to poor electrochemical performance.

In this work, a facile preparation method was developed to construct a three-dimensional architecture from a combination of nanostructured Ge particles and SWCNTs. The paper anode with good Ge nanoparticle distribution in the SWCNT network offers better electrical contact, which aids in improving the capacity and cycling stability for superior anodes in lithium ion batteries.

Experimental

Preparation of the Ge/SWCNT composite papers

To prepare the Ge/SWCNT composites, SWCNTs (purchased from UnidymTM) and 1 wt% Triton X-100 surfactant were first added into 50 mL distilled water and ultrasonically treated for 2 h. The suspensions were then mixed with 10 mL 0.15 M NaOH solutions with GeO_2 dissolved in them, followed by constant stirring for 30 min. Subsequently, the pH of the homogeneous solutions was adjusted to 7 using 0.5 M HCl. The solutions were added dropwise into 10 mL 0.32 M icy cold $NaBH_4$ solutions (~ 4 ºC) under continuous magnetic stirring, and then transferred to water baths at 60 ºC for 3 h. By using this method, three Ge/SWCNT composites were fabricated using 24, 36 and 54 mg GeO_2 precursor with the same amount of SWCNT (25mg). Specifically, three different weight GeO_2 could be theoretically converted to 17 mg, 25 mg, 38 mg Ge, calculated based on the ratio between the atomic weight of Ge (73 g/mol) and the molecular weight of GeO_2 (105 g/mol). The designed Ge percentages in the Ge/SWCNT composites above correspond to 40, 50, and 60 wt%, which are designated as Ge/SWCNT-1, Ge/SWCNT-2, and Ge/SWCNT-3, respectively. The pure Ge particles used in the characterization for reference were synthesized by the same method without SWCNTs.

To make uniform papers, the as-prepared composite suspensions were filtered through porous polyvinylidene fluoride (PVDF) membranes by positive pressure provided by a vacuum pump. As the solvent could pass through the pores, the Ge/SWCNT composites were trapped on the membrane surfaces, forming entangled mats. The mats were washed twice with distilled water, followed by ethanol to remove the remaining surfactant. The mats were allowed to dry at 60 ºC overnight in a vacuum oven. Finally, they were peeled off from the PVDF membranes, and the Ge/SWCNT composite papers were obtained. For comparison, the pure SWCNT paper was prepared by the same method without Ge precursor.

Physical characterization

X-ray diffraction (XRD, GBC-MMA) patterns were collected from the samples with Cu Kα radiation at a scanning rate of 5° min^{-1} within the 2θ range from 20° to 80°. Raman spectroscopy (JOBIN YVON HR800 Confocal system with 632.8 nm diode laser excitation) was conducted using a 300 lines mm^{-1} grating in the range of 200 to 2000 cm^{-1} at room temperature. The morphologies of the samples were examined by field emission scanning electron microscopy (FE-SEM, JEOL 7500, operated at an acceleration voltage of 1.5 kV) and transmission electron microscopy (TEM, JEOL EM 2010). The sample for TEM observation was prepared by dispersing a small piece of the Ge/SWCNT composite paper onto a holey carbon support.

Electrochemical measurements

The 1 × 1 cm square anodes were cut out from the as-prepared papers. The electrochemical cells (CR 2032 coin-type cells) were assembled in an argon gas filled glove box (Mbraun, Germany) by stacking a porous polypropylene separator between the paper anode as the working anode and the lithium foil as the counter and reference electrode. The electrolyte was 1 M $LiPF_6$ in a 50:50 (v/v) mixture of ethylene carbonate (EC) and dimethyl carbonate (DEC). The electrochemical cells were galvanostatically discharged and charged using a Land battery tester within a voltage range of 0.01 to 2.00 V at a current density of 25 mA g^{-1} and a temperature of 25 ºC. Electrochemical impedance spectroscopy (EIS) was carried out utilizing a CHI 660B electrochemical workstation.

Results and discussion

X-ray diffraction (XRD) patterns for the pure SWCNT paper, the typical Ge/SWCNT composite paper and the pure Ge powder are shown in Fig. 1(a). The diffraction peaks for SWCNTs at 2θ of 23° and 45° could be indexed as the (002) and (101) reflections [16]. The diffraction peak of the (002) diffraction is related to the typical random arrangement of CNTs, with a d_{002} of 0.38 nm calculated based on Bragg's equation. The two broad diffraction peaks for the as-prepared Ge powders indicate the nanosized structure. The diffraction pattern of the Ge/SWCNT-2 paper contains two broad peaks as well, which is presumably attributable to the overlapping of SWCNT peaks with the Ge peaks. Raman spectroscopy, as shown in Fig. 1(b), was used to further confirm the presence of Ge particles and SWCNTs in the paper. The Raman spectrum

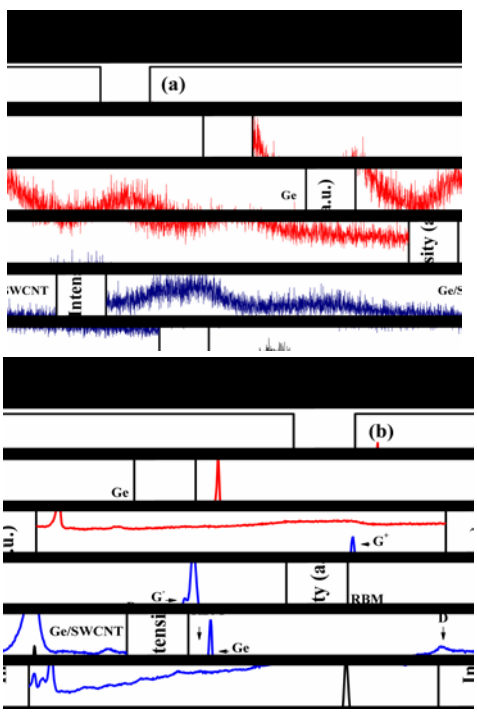

Fig. 1 XRD patterns (a) and Raman spectra (b) of the pure SWCNT paper, the Ge/SWCNT-2 paper and the pure Ge powder.

modes (RBM) region of the low frequency range below 290 cm^{-1}, the disorder induced phonon mode (D-band) at about 1306 cm^{-1}, and the tangential modes (G-band) with G^- and G^+ parts at 1554 cm^{-1} and 1593 cm^{-1}. In the Raman spectra of the composite paper, Ge bands located in 298 cm^{-1} can be identified, together with the typical SWCNT bands. This implies that the Ge/SWCNT composite papers could be successfully prepared via the method mentioned above.

FE-SEM images of the pure SWCNT paper and the Ge/SWCNT-2 paper are shown in Fig. 2. In the surface morphology of the SWCNT paper (Fig. 2(a)), the SWCNTs appear as a web of bundled and well-packed nanotubes, forming a three-dimensional network structure. Ge particles are deposited onto the SWCNT matrix in the form of both individual particles (about 10-30 nm in diameter) and clusters of particles, as shown in Fig. 2(b). The cross-sectional view of the Ge/SWCNT composite paper (Fig. 2(c) and (d)) demonstrates that it is composed of very dense, closely connected multilayers, and the total thickness is around 34 μm. The Ge nanoparticles which are distributed on the SWCNT matrix can be seen clearly. The Ge/SWCNT composite paper can be rolled up or bent freely (inset of Fig. 2c), indicating its good flexibility and mechanical property.

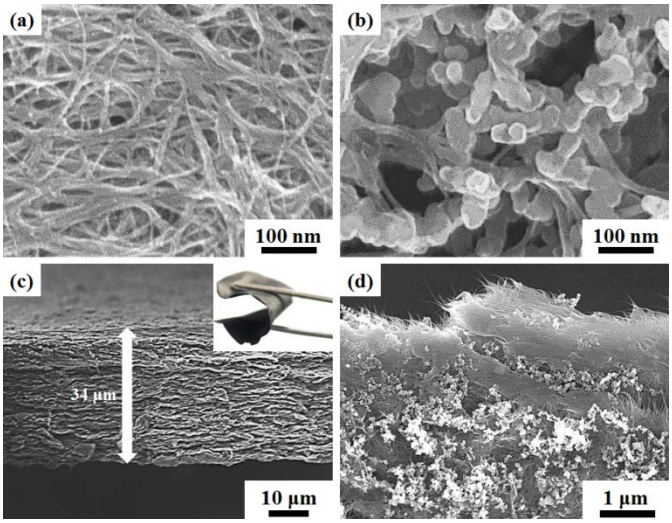

Fig. 2 FESEM images the pure SWCNT paper and the Ge/SWCNT-2 paper: top views of the pure SWCNT paper (a) and the composite paper (b); cross-sectional views of the composite paper at low magnification (c) and at high magnification (d); inset of (c) is a photograph of the composite paper.

A FE-SEM image with the corresponding energy dispersive X-ray spectroscopy (EDS) spectrum and EDS mapping images for the Ge/SWCNT-2 paper is presented in Fig. 3. The EDS spectrum (Fig. 3(b)) shows the presence of SWCNTs (C) and Ge in the Ge/SWCNT-2 paper, and the weight percentage of Ge is 32%. O is detected from the oxygenated functional groups, and Fe is the catalyst in the SWCNTs. The contents of Ge in the Ge/SWCNT-1 paper and Ge/SWCNT-3 paper were also analysed from EDS spectrum to be 22 and 45 wt%, respectively. The coloured points in the EDS mapping images (Fig. 3(b) and (c)) confirm the presence of the elements Ge and C, respectively. Furthermore, the results show the good distribution of Ge in the paper, which demonstrates that the Ge nanoparticles have been homogeneously coated onto the surface of the SWCNTs.

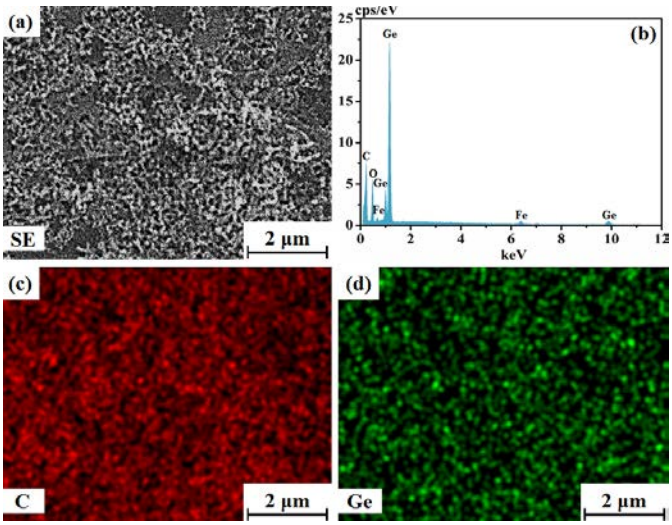

Fig. 3 FESEM image of the Ge/SWCNT-2 paper (a) with EDS spectrum (b), and corresponding EDS mapping of carbon and Ge (c, d).

TEM investigations (Fig. 4) revealed information on the morphology and structure of the Ge/SWCNT-2 paper. The low magnification image in Fig. 4(a) gives further support to the observation that the surfaces of the SWCNTs are fully covered by Ge nanoparticles. The corresponding selected area electron diffraction (SAED) pattern is shown in Fig. 4(b). The indexed fine spotty rings in the SAED correspond to structural characteristics of cubic Ge, indicating that the growth directions of the Ge nanoparticles are parallel to the (111), (220), and (311) planes (JCPDS NO.: 65-0333). The high magnification TEM image (Fig. 4(c)) clearly shows a Ge particle, the SWCNTs, and the boundary between the Ge particle and the SWCNTs. The SWCNT interplanar distance was measured to be 0.35 nm, in agreement with the (002) planes of SWCNTs. Fig. 4(d) displays lattice fringes of a typical Ge particle with a lattice spacing of 0.20 nm, corresponding to the spacing of the (220) planes of Ge.

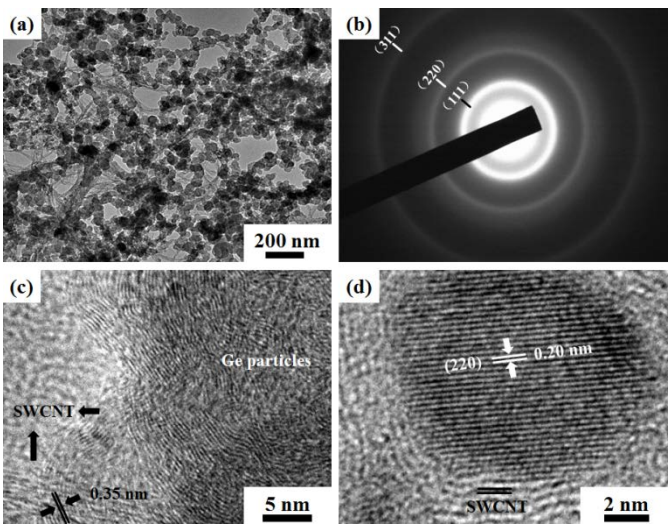

Fig. 4 TEM images obtained from the Ge/SWCNT-2 paper: low magnification image (a) and associated SAED pattern (b); high magnification TEM image showing the lattice and interface between a Ge nanoparticle and SWCNTs (c), and lattice resolved high magnification TEM image of a Ge nanoparticle on SWCNTs (d).

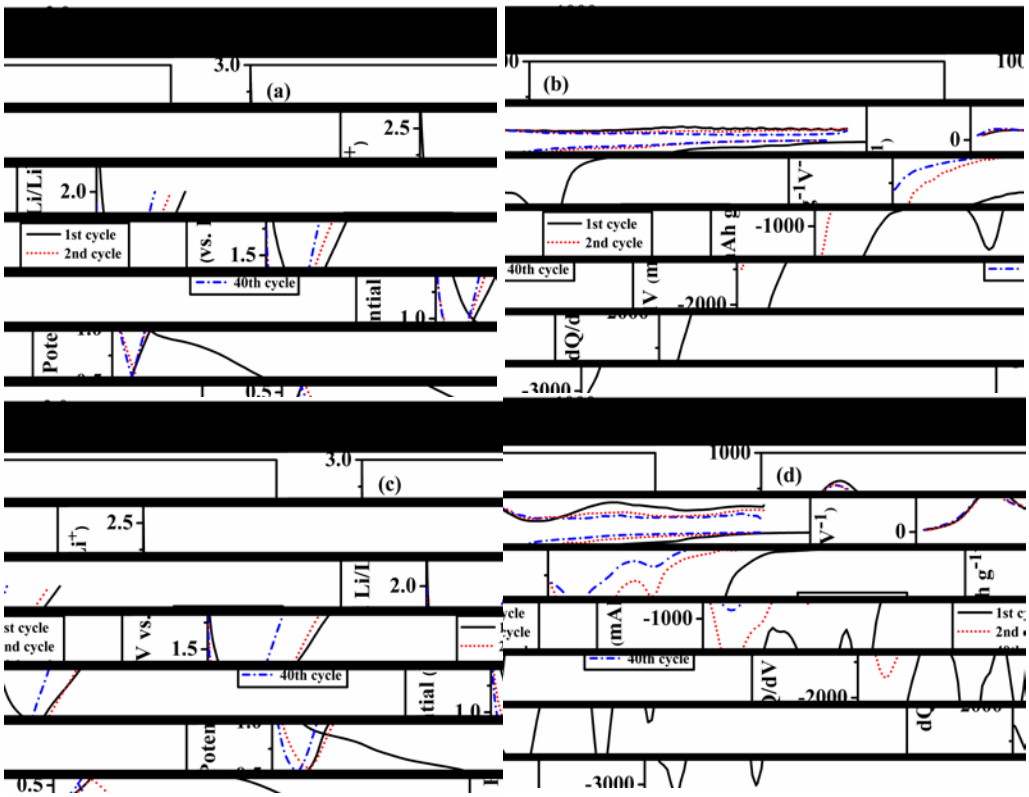

Fig. 5 Charge-discharge curves for selected cycles and their differential profiles for the pure SWCNT paper anode (a, b) and the Ge/SWCNT-2 paper anode (c, d) at current density of 25 mA g^{-1}.

Fig. 5 shows selected charge-discharge curves and their corresponding differential profiles for the pure SWCNT paper anode and the Ge/SWCNT-2 paper anode in coin cells at a current density of 25 mA g^{-1} between 0.01 and 2.00 V vs. Li/Li^+. As can be seen in Fig. 5(a), the initial discharge and charge capacities of SWCNT paper anode are 1307 and 289 mAh g^{-1}, respectively, with a coulombic efficiency of 22%. The irreversible capacity loss is mainly due to the reduction of dioxygen molecules or oxygenated functional groups on the surface of the SWCNT paper anode, the formation of a solid electrolyte interphase (SEI) layer, and further side reactions [22]. Subsequently, the pure SWCNT paper anode shows a relatively stable discharge capacity after the 2nd cycle, with an average coulombic efficiency of > 97 % up to 40 cycles. The peak at 0.8–0.9 V in the first discharge differential plot (Fig. 5(b)) corresponds to the voltage plateau in the first discharge cycle, which is associated with electrolyte decomposition and the formation of the SEI layer mentioned above. The pronounced potential below 0.4 V is attributed to the insertion of Li ions into the graphitic-type layers, which has been confirmed by previous works [23-25]. No evident peak can be traced in the following cycles, indicating the irreversible reaction. As can be seen in Fig. 5(c), the Ge/SWCNT composite paper anode exhibits an initial discharge capacity of 2024 mAh g^{-1}, with a coulombic efficiency of 33%, which is calculated based on the total mass of the paper anode. The paper anode delivers a capacity of 752 mAh g^{-1} in the second cycle, and the capacity loss mainly arises from the irreversible Li ion insertion into the paper anode and the formation of the SEI layer. Three peaks can be observed in the differential curve (Fig. 5(d)) of the first discharge cycle. The SEI layer formation occurs at the same voltage of 0.8–0.9 V as that in the SWCNT paper anode, and the other two peaks at 0.5–0.6 V and 0.1–0.2 V represent the stepwise Li alloying reaction to form different Li_xGe alloys. The differential curves of the subsequent charge cycles show a broad anodic peak at about 0.45 V, corresponding to the delithiation voltage of Li_xGe species [26-28]. Multiple sharp peaks in typical cycles still exist up to 40 cycles, suggesting that the paper anode could maintain good kinetic activity towards Li ion intercalation/deintercalation during the cycling.

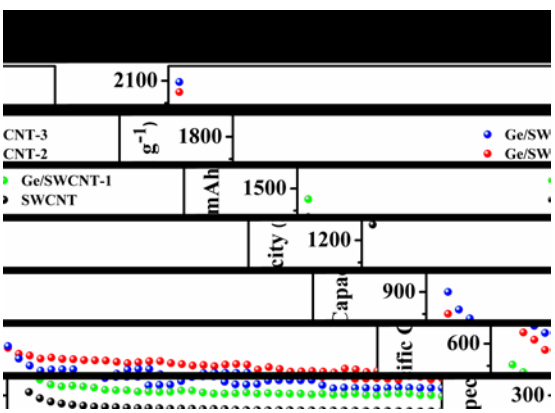

Fig. 6 Cycling stability of the pure SWCNT paper anode and different Ge/SWCNT composite papers anodes at current density of 25 mA g^{-1}.

To study the synergic effects between the conductive SWCNTs and second active phase Ge nanoparticles, the cycling stabilities of the paper anodes with various Ge weight percentages were examined as shown in Fig. 6. The discharge capacities of the Ge/SWCNT-1, Ge/SWCNT-2, Ge/SWCNT-3 paper anodes are 295, 350, 417 mAh g^{-1}after the 40 cycles, respectively. Among different Ge/SWCNT composite paper anodes, it is noted that the Ge/SWCNT-2 paper anode delivers the highest discharge capacity, which is 117% higher than that of the SWCNT paper anode (192 mAh g^{-1}). This is because that proper percentage Ge nanoparticles in the composite paper anode could serve as an electrochemically active second phase to effectively increase its discharge capacity. Moreover, mechanically robust SWCNTs in the paper anode can keep the Ge nanoparticles in good contact and mitigate the material failure caused by the volume changes of Ge nanoparticles. In addition, due to the excellent ion and electron transfer properties of SWCNTs, the accessibility to Li ions and the electrical conductivity of the paper anode could also be maintained.

The Ge/SWCNT-1 paper anode shows lower discharge capacity because of less active material Ge loading. The Ge/SWCNT-3 paper anode also delivers lower discharge capacity and unstable cycling performance, which could possibly be due to less inefficient ion and electron transfer in the paper anode and mechanical issues attributable to the volume changes of Ge particles during cycling. Therefore, the optimum Ge nanoparticle content in the composite paper anode is 32 wt%. Similar synergic effects were also observed in other composite paper anode systems [3,5].

Electrochemical impedance spectroscopy (EIS) measurements for the pure SWCNT paper anode and the Ge/SWCNT-2 paper anode were conducted using a sine wave of 10 mV amplitude over a frequency range of 100 kHz–0.01 Hz. To maintain uniformity, the impedance measurements were preformed after running charge-discharge for 5 cycles and 40 cycles in the fully charged state. The Nyquist plots and the fitting model using an equivalent circuit were compared and are depicted in Fig. 7(a), with the equivalent circuit as the inset. Both plots display one compressed semicircle in the high frequency region and a sloping line in the low frequency regime. The intercept on the Z_{real} axis in the high frequency region represents the total resistance of the electrolyte, separator, and electrical contacts (R_s). The semicircle in the high frequency range indicates the charge transfer resistance (R_{ct}), which is associated with the charge transfer reaction at the anode/electrolyte interface. The inclined line in the low frequency region represents the Warburg impedance (Z_w), related to the ion diffusion process in the anode materials [29,30].

Apparently, the diameters of the semicircles for the pure SWCNT paper anode are smaller than those for the Ge/SWCNT composite paper, indicating lower charge transfer resistance of the SWCNT paper anode after 5 (211.3Ω) and 40 cycles (279.2Ω). This result further confirms that the SWCNTs could serve as a highly conductive matrix and provide three-dimensional electric pathways for the paper anode. The Ge/SWCNT-2 paper anode also shows a low charge transfer resistance after 5 cycles (290.3 Ω). This is because good dispersion of the electrochemically active phase Ge nanoparticles at the surface of the SWCNTs could enable efficient electronic transport at the anode/electrolyte interface as well, and the SWCNTs in the paper anode possess a large

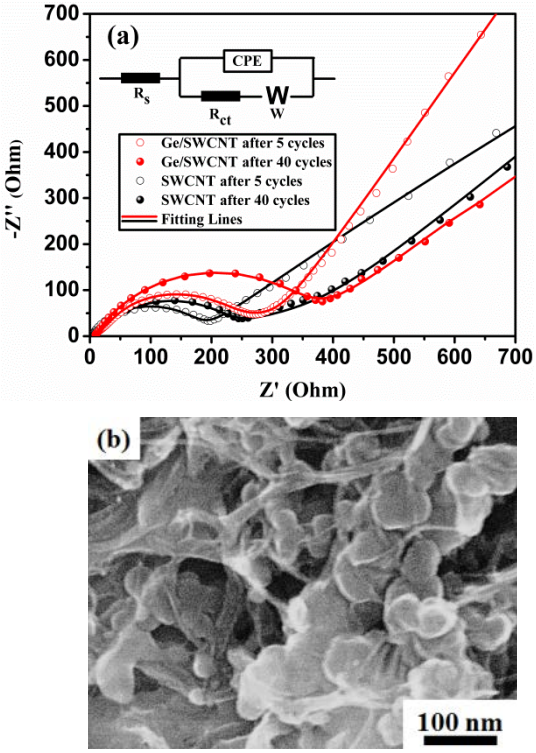

Fig. 7 Impedance spectra for the pure SWCNT paper anode and the Ge/SWCNT-2 paper anode after 5 cycles and after 40 cycles, with the inset containing the equivalent circuit model (a). FESEM image of the Ge/SWCNT-2 paper anode after 40 cycles (b).

surface area, which could relieve the volume changes of Ge nanoparticles during the charge and discharge processes. After 40 cycles, agglomerates are found to have formed on some parts of this Ge/SWCNT-2 paper anode (shown in Fig. 7(b)), and this will reduce the area of the interparticle contact between the Ge nanoparticles and the SWCNTs, resulting in higher charge transfer resistance (413.5 Ω) of the Ge/SWCNT composite paper anode.

Conclusions

In the Ge/SWCNT composite papers, SWCNTs form robust three-dimensional architectures with nanosized Ge particles uniformly deposited on the surface of SWCNTs. Compared with previous works of SWCNT-based paper anodes, the Ge/SWCNT composite paper anode with a relatively low active phase content (32 wt%) was synthetized by a simpler and low temperature route, and delivers a satisfactory reversible discharge capacity of 417 mAh g^{-1} after 40 cycles. The improved electrochemical performances of the Ge/SWCNT composite paper anode can be attributed to the good distribution of high capacity Ge in the SWCNT network, which increases the anode's conductivity, provides void space to buffer the Ge nanoparticle volume changes, so as to enable more efficient channels for the lithium insertion and deinsertion during discharge–charge cycles.

Acknowledgements

Jun Wang is grateful to the China Scholarship Council (CSC) for scholarship support. The authors are grateful for funding from the Australian Research Council (ARC) under the ARC Centre of Excellence Program, and also acknowledge the use of facilities in the UOW Electron Microscopy Centre. Many thanks are owed to Dr. Tania Silver for critical reading of the manuscript.

Notes and references

[a] Institute for Superconducting and Electronic Materials, University of Wollongong, NSW 2500, Australia. E-mail: jiazhao@uow.edu.au; hua_liu@uow.edu.au; Fax: +61 2 4221 5731; Tel: +61 2 4298 1478.
[b] ARC Center of Excellence for Electromaterials Science, University of Wollongong, NSW 2500, Australia.

1 A. S. Arico, P. Bruce, B. Scrosati, J. M. Tarascon and W. Van Schalkwijk, *Nat. Mater.*, 2005, **4**, 366.
2 D. Liu and G. Cao, *Energy Environ. Sci.*, 2010, **3**, 1218.
3 J. Z. Wang, L. Lu, M. Lotya, J. N. Coleman, S. L. Chou, H. K. Liu, A. I. Minett and J. Chen, *Adv. Energy Mater.*, 2013, **3**(6), 798.
4 L. Hu and Y. Cui, *Energy Environ. Sci.*, 2012, **5**, 6423.
5 X. L. Jia, Z. Chen, A. Suwarnasarn, L. Rice, X. L. Wang, H. Sohn, Q. Zhang, B. M. Wu, F. Wei and Y. F. Lu, *Energy Environ. Sci.*, 2012, **5**, 6845.
6 L. Noerochim, J. Z. Wang, D. Wexler, M. M. Rahman, J. Chen and H. K. Liu, *J. Mater. Chem.*, 2012, **22**, 11159.
7 J. Z. Wang, S. L. Chou, J. Chen, S. Y. Chew, G. X. Wang, K. Konstantinov, J. Wu, S. X. Dou and H. K. Liu, *Electrochem. Commun.*, 2008, **10**, 1781.
8 S. Y. Chew, S. H. Ng, J. Z. Wang, P. Novak, F. Krumeich, S. L. Chou, J. Chen and H. K. Liu, *Carbon*, 2009, **47**, 2976.
9 S. H. Ng, J. Z. Wang, Z. P. Guo, J. Chen, G. X. Wang and H. K. Liu, *Electrochim. Acta*, 2005, **51**, 23.
10 B. J. Landi, M. J. Ganter, C. D. Cress, R. A. DiLeo and R. P. Raffaelle, *Energy Environ. Sci.*, 2009, **2**, 638.
11 J. Wang, L. L. Li, C. L. Wong and S. Madhavi, *Nanotechnology*, 2012, **23**, 1.
12 S. L. Chou, Y. Zhao, J. Z. Wang, Z. X. Chen, H. K. Liu and S. X. Dou, *J. Phys. Chem. C*, 2010, **114**, 15862.
13 K. Fu, O. Yildiz, H. Bhanushali, Y. X. Wang, K. Stano, L. G. Xue, X. W. Zhang and P. D. Bradford, *Adv. Mater.*, 2013, **25**, 5109.
14 G. M. Zhou, D. W. Wang, P. X. Hou, W. S. Li, N. Li, C. Liu, F. Li and H. M. Cheng, *J. Power Sources*, 2012, **22**, 17942.
15 Z. Y. Cao and B. Q. Wei, *J. Power Sources*, 2013, **241**, 330.
16 L. Noerochim, J. Z. Wang, S. L. Chou, D. Wexler and H. K. Liu, *Carbon*, 2012, **50**, 1289.
17 J. W. Qin, Q. Zhang, Z. Y. Cao, X. Li, C. W. Hu, B. Q. Wei, Nano Energy, 2013, 2, 733-741.
18 D. J. Xue, S. Xin, Y. Yan, K. C. Jiang, Y. X. Yin, Y. G. Guo and L. J. Wan, *J. Am. Chem. Soc*., 2012, **134**, 2512.
19 K. H. Seng, M. H. Park, Z. P. Guo, H. K. Liu and J. Cho, *Nano Lett.*, 2012, **51**, 5657.
20 G. Jo, H. Choi, H. Ahn and M. J. Park, *Chem. Commun*., 2012, **48**, 3987.
21 R. A. DiLeo, M. J. Ganter, B. J. Landi and R. P. Raffaelle, *J. Mater. Res.*, 2010, **25**(8), 1411.
22 S. Y. Chew, S. H. Ng, J. Z. Wang, P. Novák, F. Krumeich, S. L. Chou, J. Chen and H. K. Liu, *Carbon*, 2009, **47**, 2976.
23 J. Y. Eom and H. S. Kwon, *Mater. Chem. Phys*., 2011, **126**, 108.
24 H. S. Oktaviano, K. Yamada and K. Waki, *J. Mater. Chem.*, 2012, **22**, 25167.
25 W. X. Chen, J. Y. Lee and Z. L. Liu, *Carbon*, 2003, **41**, 959.
26 A. M. Chockla, M. G. Panthani, V. C. Holmberg, C. M. Hessel, D. K. Reid, T. D. Bogart, J. T. Harris, C. B. Mullins and B. A. Korgel, *J. Phys. Chem. C*, 2012, **116**, 11917.
27 C. Zhong, J. Z. Wang, X. W. Gao, D. Wexler and H. K. Liu, *J. Mater. Chem. A*, 2013, **1**, 10798.
28 S. Yoon, C. M. Park and H. J. Sohn, *J. Electrochem. Soc.*, 2008, **11**(4), A42.
29 Z. J. Zhang, J. Z. Wang, S. L. Chou, H. K. Liu, K. Ozawa and H. J. Li, *Electrochim. Acta*, 2013, **108**, 820.
30 X. W. Gao, J. Z. Wang, S. L. Chou and H. K. Liu, J. Power Sources, 2012, 220(15), 47.